Comparison of soil damping methods for offshore wind turbines

Panagoulias, S.; Nernheim, A.; Voges-Espelage, P.

DOI
10.3723/SHDJ4954

Publication date
2023

Document Version
Final published version

Published in
Offshore Site Investigation Geotechnics 9th International Conference Proceeding

doi:10.3723/SHDJ4954

Comparison of soil damping methods for offshore wind turbines

S. Panagoulias
Delft University of Technology, Delft, the Netherlands
Siemens Gamesa Renewable Energy, The Hague, the Netherlands

A. Nernheim & P. Voges-Espelage
Siemens Gamesa Renewable Energy, Hamburg, Germany

ABSTRACT: Sound evaluation of soil damping is of great importance for the optimised design of offshore wind turbine support structures. As practice indicates, design optimisation of the support structure often leads to fatigue-driven structural components, especially at the monopile foundation. Saving steel material is important for the economic feasibility of the project, while satisfying fabrication, transportation, and installation requirements. Conventionally, the baseline/background damping consists of steel material, hydrodynamic and soil damping. Design experience indicates that soil damping contribution to the overall baseline damping is significant, especially in case of strong non-linear soil response. This study employs an analytical and a numerical method to evaluate soil damping under realistic project conditions. Results indicate that the analytical method offers a sound basis for fatigue-oriented soil damping assessments, especially at the initial stages of the project.

1 Introduction

The importance of soil damping on the fatigue assessment of the support structures of offshore wind turbines (OWTs) is acknowledged by current design standards (DNV, 2019; 2021). This is particularly true for the monopile-founded OWTs due to the "monolithic" nature of the system, which creates a strong interaction between the response of the foundation and the superstructure. Under typical environmental loading conditions related to the action of wind and waves, the frequency content of interest lies below approximately 0.3Hz. Therefore, it is the fundamental eigenfrequency of the system, in the range of 0.1-0.25Hz for large OWTs, that plays a critical role on the system's dynamic response.

Damping is crucial for both the extreme loads under the Ultimate Limit State (ULS) conditions and the fatigue loads under the Fatigue Limit State (FLS) conditions. Safe and optimised design of the fatigue-driven parts of the support structure highly depends on the damping associated to the fundamental eigenfrequency.

Various sources of damping are acting upon OWTs, most commonly consisting of passive mechanical systems, e.g., tuned-mass or slosh dampers, and physical sources. The latter includes what is known as "baseline damping" (or "background damping") and includes the aerodynamic damping (arising from the presence of the rotor), structural damping, hydrodynamic damping (viscous and radiation), and soil damping (material/hysteretic, geometric/radiation and hydro-mechanical) (IEC, 2019). The present paper only focuses on soil damping, with emphasis on the material/hysteretic component. The contribution of the radiation component becomes significant only if the system's vibrating frequency is higher than the cut-off frequency of the soil medium, typically around 1Hz (Damgaard et al., 2013; Carswell et al., 2015). Given the low frequency of the first mode of the oscillating support structure, the contribution of the geometric damping to the total soil damping is considered negligible in the present study, assuming quasi-static soil response (Chen and Duffour, 2018).

Malekjafarian et al. (2021) present a review of damping for monopile-supported OWT, with special attention to soil damping, summarizing a big number of numerical and experimental studies on the topic. The reported values of soil damping widely vary on average from 0.15% to 1.5% of critical (about 1%-9% logarithmic decrement (LD)), depending on the soil material type (sand-only, clay-only, layered), the properties of the structure and the loading characteristics. The dependency of soil damping on the loading amplitude is also highlighted by Kementzetzidis et al. (2019). Stuyts et al. (2022) presented a comparison between derived soil damping values from measured data and numerical models for a Belgian offshore wind project, highlighting the need for advanced soil reaction models for sound evaluation.

The impact of soil damping to the fatigue damage of OWTs is also widely acknowledged. Depending on the assumed turbine characteristics, support structure configuration, operational conditions, and the employed soil-structure interaction model, increased soil material damping could lead to considerable reduction of fatigue damage (Damgaard et al., 2015; Schafhirt et al. 2016).

This paper presents a comparison between an analytical and a numerical method for the evaluation of soil hysteretic damping. A case-study of a state-of-the-art large OWT is considered, under typical environmental conditions offshore North Sea. Section 2 provides an overview of the input soil conditions and the properties of the analysed system. Section 3 presents the adopted methodologies to evaluate soil damping, while the obtained results are discussed in Section 4. Conclusions are summarized in Section 5.

2 Input conditions

2.1 *Soil properties overview*

The offshore wind farm under consideration is located in the North Sea. The soil conditions are dominated by medium dense to dense sands, with inclusions of silty or slightly clayey material in thin soil layers. Consequently, the encountered soil profiles are quite stiff and of high strength. While such competent soil conditions allow for optimised foundation designs in terms of dimensions and steel mass, they might also lead to a limited amount of soil damping being activated, which has negative impact on fatigue.

Soil characterisation is based on data from in-situ cone penetration tests (CPTs), supplemented with laboratory test data, both static and cyclic, conducted on specimens from a big number of boreholes across the entire wind farm.

Geotechnical interpretation of the soil conditions is conducted by making use of the CPT data, using industry-standard empirical correlations. The stratification is based on the Normalised Soil Behaviour Type (SBTn) according to Robertson and Cabal (2015). The effective internal angle of friction for sand (φ') is derived using the procedure described by Schmertmann (1978), in combination with the relative density assessment presented by Baldi et al. (1986). The undrained shear strength of the clay layers (s_u) is calibrated using geotechnical-unit (geo-unit) specific parameters based on the available laboratory triaxial tests. The small strain shear modulus (G_0) is derived from the CPT data using the procedure described by Rix and Stokoe (1991). Furthermore, seismic CPTs (SCPTs) have been used to correlate stiffness parameters with in-situ data for the sand layers. For clay layers, the correlation published by Mayne and Rix (1993) is applied. Table 1 presents the results of the geotechnical interpretation for the location selected for this study.

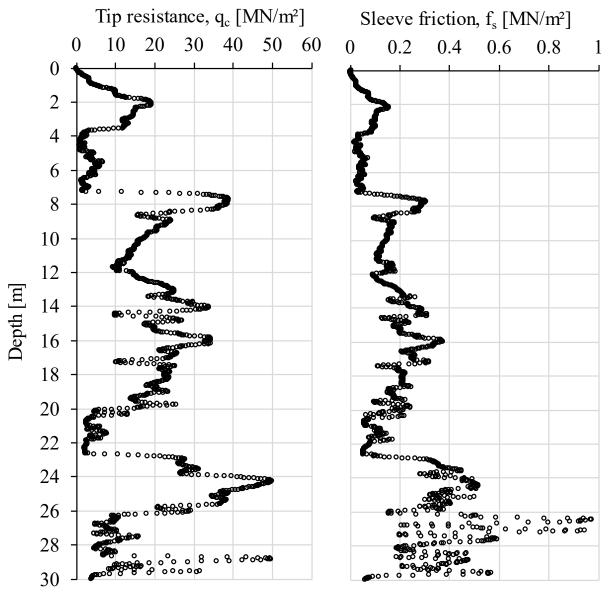

Figure 1 CPT data for the selected design location

Table 1. Main soil parameters of the selected location. z_{layer} = depth of the soil layer below ground level (top to bottom), γ' = submerged unit weight, G_0 = small-strain shear modulus, φ' = internal friction angle, s_u = undrained shear strength; PI = plasticity index

z_{layer}	Geo-unit	γ'	K_0	G_0	φ'	s_u	PI
(m)	(-)	(kN/m³)	(-)	(MPa)	(°)	(kPa)	(%)
0.0-1.0	A	7	0.4	40	40	-	-
1.0-1.8	B	9	0.3	58	43	-	-
1.8-3.6	B	10	0.3	84	44	-	-
3.6-6.0	C1	8	1.2	87	32	-	-
6.0-7.3	C1	8	1.2	94	-	133	12
7.3-8.4	C2	11	0.9	109	44	-	-
8.4-12.5	F	10	1.1	137	38	-	-
12.5-20.4	F	11	1.0	181	38	-	-
20.4-22.7	F	9	0.9	164	-	152	15
22.7-25.9	F	12	0.8	240	40	-	-
25.9-28.7	G	11	0.8	321	-	576	18
28.7-30.0	G	11	0.8	267	39	-	-

2.2 *Support structure geometry*

The support structure consists of a tower founded on a monopile, without a transition piece. The tower has a bottom outer diameter of 7.5m, which is equal to the monopile's top diameter. At mudline, below the conical section, the monopile's outer diameter equals 9.5m. The penetration depth below ground level is 26m, resulting in an embedment ratio of 2.74. The water-depth with respect to the Lowest Astronomical Tide (LAT) equals 32m.

2.3 *Soil reaction curves*

The analytical method used in the present study to evaluate soil damping (see Section 3.1) makes use of a one-dimensional (1D) Finite Element (FE) model in which soil reaction is formulated via a set of lateral-only nonlinear soil reaction curves, in the form of distributed force-displacement springs (*p-y* springs).

The employed formulation constitutes an enhanced version of the API (2014) codified equations for the sand layers and the Jeanjean (2009) equations for the clay layers. The p-y springs are calibrated to fit the results of a static push-over analysis in a three-dimensional (3D) FE model in terms of lateral deflection, rotation and curvature of the embedded part of the monopile. Further information about the employed methodology is given by Panagoulias et al. (2023). Cyclic degradation is applied to the calibrated soil springs following API (2014). Scour-related effects are not considered in this study.

It is acknowledged that recent studies indicate advantage of including additional soil reaction components in the 1D FE model, related to the distributed and based moment reactions, for the modelling of soil-monopile interaction (Byrne et al., 2019). However, the applied calibration method of the lateral-only soil reaction curves, in general, but also in this study in particular, results in sufficiently accurate match between the 1D and the 3D FE models. Besides, the employed analytical method for the soil damping assessment is originally based on lateral-only soil reactions (see Section 3.1)

2.4 *Damping laboratory test data*

Relevant laboratory test data from all geo-units present at the selected location (see Table 1) are used the damping assessment. Indicatively, Figure 2 presents data for the cohesionless geo-unit B of soil layer 2, in terms of stiffness degradation (Figure 2a) and soil material damping (Figure 2b). Geo-unit B is located at a shallow depth (see Table 1) and, therefore, it is expected to have a considerable impact on the resulting soil damping. Resonant Column (RC) tests and Cyclic Direct Simple Shear (CSS) tests have been used to calibrate the stiffness degradation and the soil material damping curves. Sections 2.5 and 3.2.2 further discuss the calibration process of the soil material damping curves.

2.5 *Soil material damping assessment*

Geo-unit specific soil material damping curves are calibrated using Equation 1. The derived fitting parameters *a*, *b*, *c* and *d* are reported in Table 2 per geo-unit.

$$\beta_{geo-unit} = \frac{a}{1+exp[b\cdot(log(\gamma)+c)]} + d \qquad (1)$$

where $\beta_{geo\text{-}unit}$ = shear strain-dependent soil material damping (-), a, b, c, d = fitting parameters to the geo-unit specific data (see Table 2) and γ = shear strain (-).

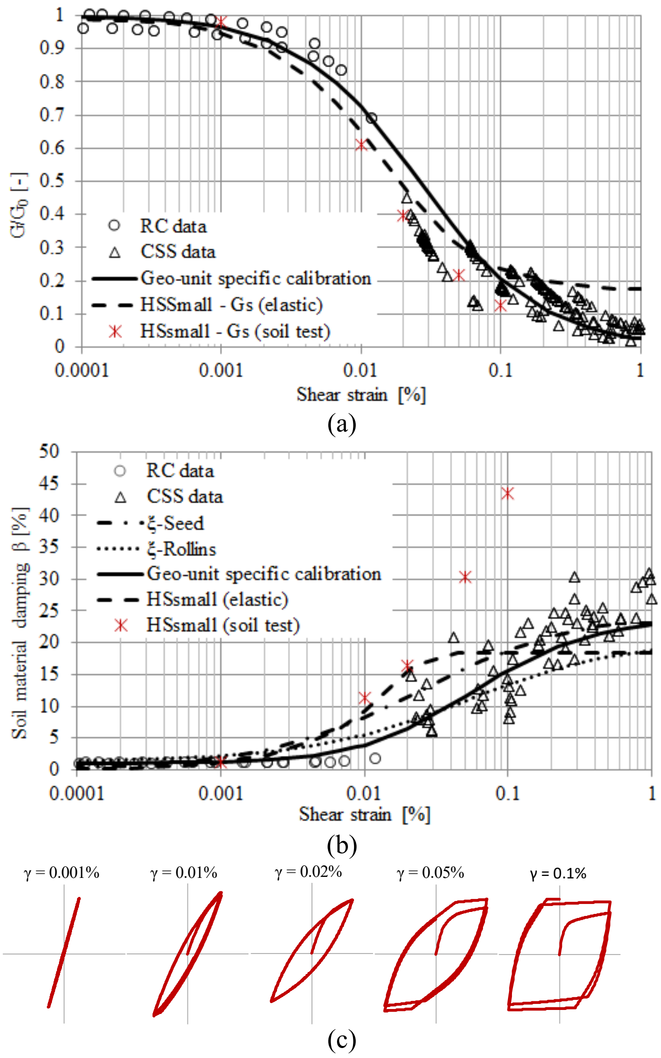

Figure 2 Stiffness degradation (a) and soil material damping (b) laboratory test data and curves for the cohesionless geo-unit B of the soil layer 2. Qualitative cyclic stress-strain response of a soil element (c), corresponding to the HSsmall data points (PLAXIS soil test) for five different (cyclic) shear strain levels

Table 2. Overview of the fitting parameters to Equation 1 for the geo-units of the selected location (see Table 1)

Geo unit	Parameter *a* (-)	Parameter *b* (-)	Parameter *c* (-)	Parameter *d* (-)
A	23	-2.5	1.2	1
B	23	-2.5	1.2	1
C1 - Sand	22	-2.5	0.9	1
C1 - Clay	26	-2	1.1	0.7
C2	22	-2.5	0.9	1
F - Sand	22	-2.5	0.9	1
F - Clay	21	-2	0.8	2.5
G - Clay	21	-2	0.8	2.5

To provide a comparison with empirical correlations well-established in literature, two additional scenarios are assessed for the soil material damping curves (Figure 2). First, a case using the formulation according to Seed et. al (1986) for cohesionless and Vucetic and Dobry (1991) for cohesive soil types. Second, a case using Rollins et al. (1998) for cohesionless and Vucetic and Dobry (1991) for cohesive soil types. Due to the limited presence of cohesive layers in the selected profile (see Table 1), no further variation of the clay formulation is considered. Other more recent formulations suggested by literature (e.g., Darendeli, 2001) could be investigated additionally, but the combinations above are considered sufficient to draw meaningful conclusions.

Figure 2b presents a comparison between the laboratory test data available for geo-unit B against the geo-unit calibrated soil material damping curve (Equation 1 and Table 2) and the two literature-based correlations described above for cohesionless material. The geo-unit calibrated curve follows very well the laboratory test data. The damping curve given by Rollins et al. (1998) is close to the laboratory data (and therefore the geo-unit calibrated curve) only at the medium strains range, while the curve by Seed et al. (1986) overestimates soil material damping. This difference has a direct effect on the soil damping (see Section 4). Is it noted that similar trends were also found in all other geo-units.

2.6 *Loading conditions*

The assessment of soil damping at different loading conditions is done indirectly. A range of mudline deflections is considered which can result from environmental loading of different amplitude and frequency. Based on the current design experience, a range from about 1mm to about 30mm is examined. Typically, mudline deflections at the lower part of this span are associated with the FLS loading conditions, while the ULS loads lead to higher displacement levels, towards the upper part of the span.

3 **Methodology**

3.1 *Analytical damping evaluation method*

The analytical method reported by Cook & Vandiver (1982), is used to estimate the soil damping in the first vibration mode. Under the assumption that damping can be modelled using equivalent linear dashpots, the soil damping is given by Equation 2.

$$\xi_{soil} = \frac{\Xi_{soil}}{2\omega_1 M} \tag{2}$$

where Ξ_{soil} = the modal soil damping (-), ω_1 = the undamped modal natural angular frequency of the first mode (rad/s), M is the system's total modal mass including all added masses (kg) and ξ_i is the modal soil damping ratio (-).

The hysteretic part of the soil damping in Equation 2 is given by Equation 3.

$$\xi_{soil,hys} = \frac{W_D}{4\pi W_S} = \frac{1}{M\omega_1^2}\sum_{i=1}^{n}\beta_{(z_i)}K_{s(z_i)}\psi_{(z_i)}^2 \tag{3}$$

where W_D = strain energy dissipated in the soil per cycle (J), W_S = peak elastic energy stored in the soil during a cycle (J), β = soil material damping (-), K_S = initial stiffness of the soil reaction (N/m), ψ = mode shape value (m), z = depth below ground level (m) and i = 1st to nth level below ground level (-).

The soil material damping β denotes the fraction of the strain energy that is dissipated per loading cycle in the soil medium. In practice, β is obtained via the soil material damping curves and is soil layer specific. Section 2.5 provides an overview of the employed curves based on project-specific calibration and correlations from literature.

To compute soil damping at various mudline deflection levels (see Section 2.6) using Equation 3, the fundamental mode shape is linearly scaled based on the target displacement at mudline. A correlation between the spatially averaged shear strains γ of the soil elements around the pile and the lateral pile displacement y is required. For that purpose, the formulation proposed by Kagawa & Kraft (1980) is used, given by Equation 4. This formulation has been originally developed for long and slender piles, but it has been adopted as a reasonable approximation in other monopile-related damping studies (Ishihara and Wang, 2019; Stuyts et al., 2022). The authors acknowledge the potential inaccuracy introduced by Equation 4 to the hysteretic soil damping derived by Equation 3. This is further discussed in Section 4.

$$\gamma \approx \frac{1+v}{2.5D} y \tag{4}$$

where v = the Poisson's ratio of the soil layer (-) and D = the outer pile diameter (m).

3.2 *Numerical damping evaluation method*

3.2.1 *The finite element modelling*

The Free Vibration (FV) method is used to evaluate soil damping numerically. The method requires an accurate model representation of the support structure, with accurate mass and stiffness distribution. Furthermore, a suitable constitutive relationship is needed to model the cyclic soil response, and therefore, energy dissipation through soil. The FV analyses presented in this study are carried out in the FE software PLAXIS 3D (Brinkgreve et al, 2021). The FV is used to derive the system's damping attributed solely to soil damping. This is achieved by excluding all other sources of baseline damping in the modelling configuration, i.e., structural and hydrodynamic.

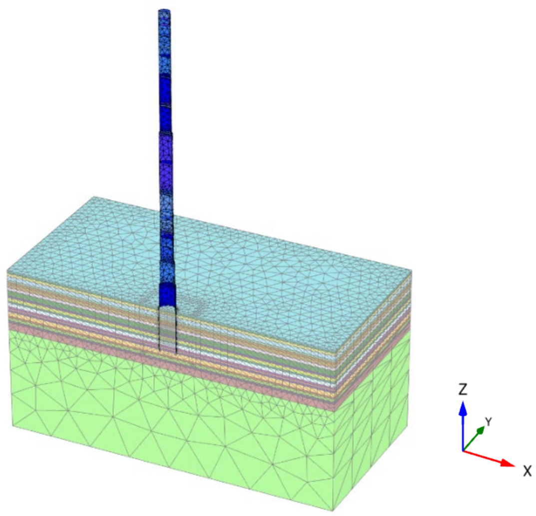

Figure 3. The FE model used for the FV analyses in PLAXIS

Figure 3 depicts the 3D FE model used for the numerical analyses. Dynamic boundary conditions are applied at the model boundaries. Viscous dashpots are assigned to "side" model boundaries in normal and tangential directions (Lysmer and Kuhlemeyer, 1969). A fully reflective dynamic boundary is assigned at the plane of symmetry (y_{min}). The boundaries are also placed further away from the vibrating structure to minimize interaction with potentially reflected waves.

To properly capture the mass and stiffness distribution of the support structure different plate materials are used to simulate different structural properties, as illustrated in Figure 3. Point masses representing flanges and other local mass components (e.g., internals, platforms, passive damping systems) are modelled with additional plate elements of representative density and geometry.

The soil stress state is initiated according to the soil material properties summarised in Table 1. The structure is wished in place and loaded laterally at the rotor-nacelle assembly (RNA) level. Afterwards, the structure is let to vibrate freely in a dynamic numerical analysis.

The FE mesh is adjusted to satisfy space discretisation and computation accuracy criteria. The shear wave velocity (V_s) increases with depth (according to the G_0 profile in Table 1). Assuming a maximum frequency of interest equal to approximately 0.5Hz (see Section 1), the minimum designated wavelength is calculated at the top and bottom of the model. Accounting for approximately 10 nodes per wavelength (Watanabe et al., 2017), the theoretically suitable maximum grid/nodal spacing is 50m at the top and 100m at the bottom. Furthermore, to accurately capture the response of the system, mesh refinement is applied at the vicinity of the structure. To maintain as low computation time as possible, mesh is properly adjusted to satisfy the criteria above without the presence of heavily distorted elements. The resulting mesh consists of about 95 000 10-noded tetrahedral elements, with minimum, average and maximum element size of 0.3m, 5.5m, and 38m (at the bottom of the model) respectively.

Constant time-stepping size is automatically determined by the PLAXIS kernel (Brinkgreve et al, 2021) to ensure numerical accuracy and stability. The Newmark Average Acceleration time integration scheme is applied with $\gamma_N = 0.5$ and $\beta_N = 0.25$. Therefore, zero numerical damping is introduced to the analysis.

Applying the load at the RNA level before releasing triggers mainly the first vibration mode. The time series of the displacement at the RNA level is analysed to derive the system's damping based on the logarithmic decrement method (Chopra, 1995). The corresponding mudline pile deflection is approximated as peak-to-peak average value over a certain number of cycles.

The vibration frequency and deflection shape are found to be very close to the fundamental eigen frequency and first mode shape of the system derived by modal analysis. Due to the low frequency content of the dynamic response (see Section 1) the contribution of radiation damping is assumed to be negligible. As there is no other source of damping than soil, the peak-to-peak soil hysteretic damping is derived via Equation 5.

$$\xi_{soil,hys} = \ln\left(\frac{u_k}{u_{k+1}}\right) = \frac{2\pi\zeta_{soil,hys}}{\sqrt{1-\zeta_{soil,hys}^2}} \approx 2\pi\zeta_{soil,hys} \quad (5)$$

where $\xi_{soil,hys}$ = soil hysteretic damping (LD); $\zeta_{soil,hys}$ = soil hysteretic damping (% of critical); u_k and u_{k+1} = the peak displacement at the peaks/troughs k and $k+1$ respectively.

3.2.2 *Calibration of the constitutive model*

The Hardening Soil with small-strain stiffness (HSsmall) constitutive model of PLAXIS is used to simulate the cyclic soil response and estimate the associated soil hysteretic damping (Brinkgreve et al., 2021). Sandy and clayey soil layers are modelled as drained and undrained respectively (Table 1). Note that the soil damping formulation in HSsmall is independent of the loading frequency since it is based on a time-independent stress-strain constitutive relationship. However, this is deemed an acceptable simplification for the low-frequency quasi-static cyclic loading of the problem at hand.

Under cyclic loading, the HSsmall model follows the Masing's rules. Stiffness decreases from the initial small-strain shear stiffness (G_0) with increasing shear strain γ. Under load reversal (unloading) the stiffness re-initiates from G_0. If upon stiffness degradation the unloading-reloading stiffness G_{ur} is reached, the associated damping does not increase any further. However, the soil material damping as given by the constitutive relations of the HSsmall model only applies while the material behaviour remains elastic. Damping further increases once (hardening) plasticity takes place (Brinkgreve et al., 2007). This effect is illustrated in Figure 2b where the HSsmall elastic formulation results are presented together with the results from the PLAXIS Soil Test application (at five different shear strain levels). The elastic formulation is in good agreement with Soil Test up to a strain approximately equal to 0.02-0.05%. In this range hardening plasticity starts occurring as it is qualitatively depicted in Figure 2c.

The calibration process suggested by Brinkgreve et al. (2021) is followed to estimate the HSsmall model stiffness parameters (assuming $E_{50,ref} = E_{oed,ref} = E_{ur,ref}/3$, with stress-level dependency, m = 0.5), and the values of G_{ur}, based on the empirical correlation of Alpan (1970). As shown in Figure 2 for the geo-unit B (soil layer 2) in particular, the selected G_{ur} value imposes a lower "cap" to the shear stiffness and an upper "cap" to the soil material damping, under elastic soil behaviour. The unloading-reloading stiffness could be selected such that the observed "cap" is better adjusted to fit the lab data at higher strains, however that would lead to greater overestimation of the soil material damping in the medium strain regime. For the sake of conservatism and transparency on the calibration process the authors have chosen not to deviate from the calibration process suggested by Brinkgreve et al. (2021). Stiffness degradation and soil material damping also depend on the threshold shear strain $\gamma_{0.7}$ at which the shear modulus reduces to about 70% of G_0. This parameter has been calculated by Equation 6 (Brinkgreve et al., 2021). The adopted calibration process results in very good fitting of the stiffness degradation curve to the laboratory test data (Figure 2a). However, the soil material damping is overestimated overall (Figure 2b).

$$\gamma_{0.7} = \frac{1}{9G_0}[2c'(1+\cos(2\phi')) - \sigma'_1(1 + K_0)\sin(2\phi')] \quad (6)$$

where c' = effective cohesion, φ' = internal friction angle, σ'_1 = effective vertical stress (compression is negative) and K_0 = earth pressure coefficient at rest.

4 **Results**

Figure 4 illustrates the fitting of the exponential function to the lateral displacement obtained at the RNA level from one of the 3D FE analyses. Both top (max/$x_{positive}$ displacement) and bottom (min/$x_{negative}$ displacement) peaks are considered. Soil damping equal to 1.9%LD corresponds to the presented case, related to a mudline deflection of about 12mm. Time is normalised by multiplying with the system's vibration frequency f_1.

Figure 5 presents a comparison of the computed soil damping between the analytical method, considering the three variations in the soil material damping curves discussed in Section 2.5, and the FV method. The values are presented in %LD, which is commonly used in the offshore wind industry. The two combinations of the literature-based soil material damping correlations lead to higher soil damping results. This outcome is reasonable considering the results presented in Figure 2b. A very good agreement is observed between the project-specific (i.e., geo-unit calibrated) analytical results and the FV results for mudline deflections up to approximately 5mm. This is a range of displacements usually encountered at FLS loading conditions. For higher displacements, FV leads to almost linearly increasing values of soil damping, while the project-specific analytical method indicates a parabolic trend.

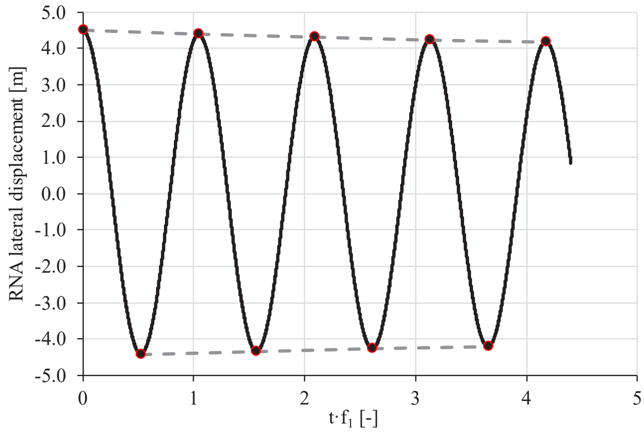

Figure 4. Fitting of exponential functions to the lateral displacement at RNA level for an indicative FV analysis

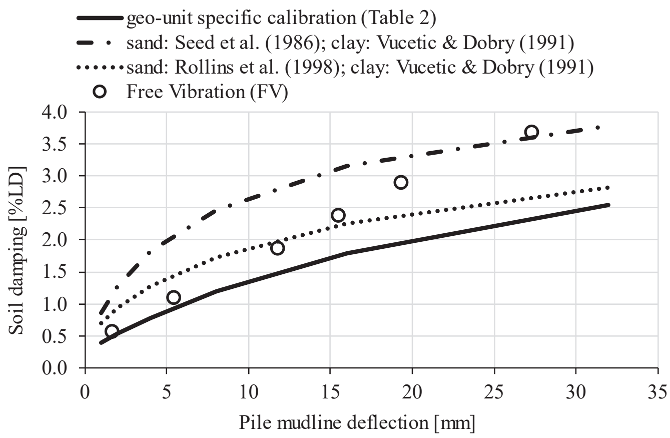

Figure 5. Comparison of the obtained values (%LD) for the soil damping between the analytical and the numerical (FV) methods

To gain better understanding about this mismatch at higher displacements, Figure 6 illustrates a comparison between the shear strains extracted from the 3D FE model and the values obtained with Equation 4 (which are used in the analytical method – see Section 3.1), for three different mudline deflections, 2mm, 6mm and 12mm. The maximum shear strain of the soil elements in the 3D FE model, is calculated as $\gamma = \varepsilon_1\text{-}\varepsilon_3$, where ε_1 and ε_3 = major and minor principal strains. The 3D-derived shear strains are presented in three groups in relation to the distance of the stress points from the outer pile diameter (D); less than 0.1D (i.e., almost 1m), between 0.1D and 0.5D and beyond 0.5D.

As discussed in Section 3.2.1 the soil material damping values resulting from the HSsmall model formulation (including plasticity) are considered realistic if shear strains remain lower than a threshold of approximately 0.02-0.05%. In addition, Equation 4 indicates that shear strains of 0.02-0.05% at mudline would correspond to displacements of about 3-7mm. These observations indicate the FV results could be treated as sound for the mudline displacement of 2mm (Figure 5 and Figure 6a) but become questionable for the mudline displacement of 5mm (Figure 5 and Figure 6b) and beyond (Figure 5 and Figure 6c).

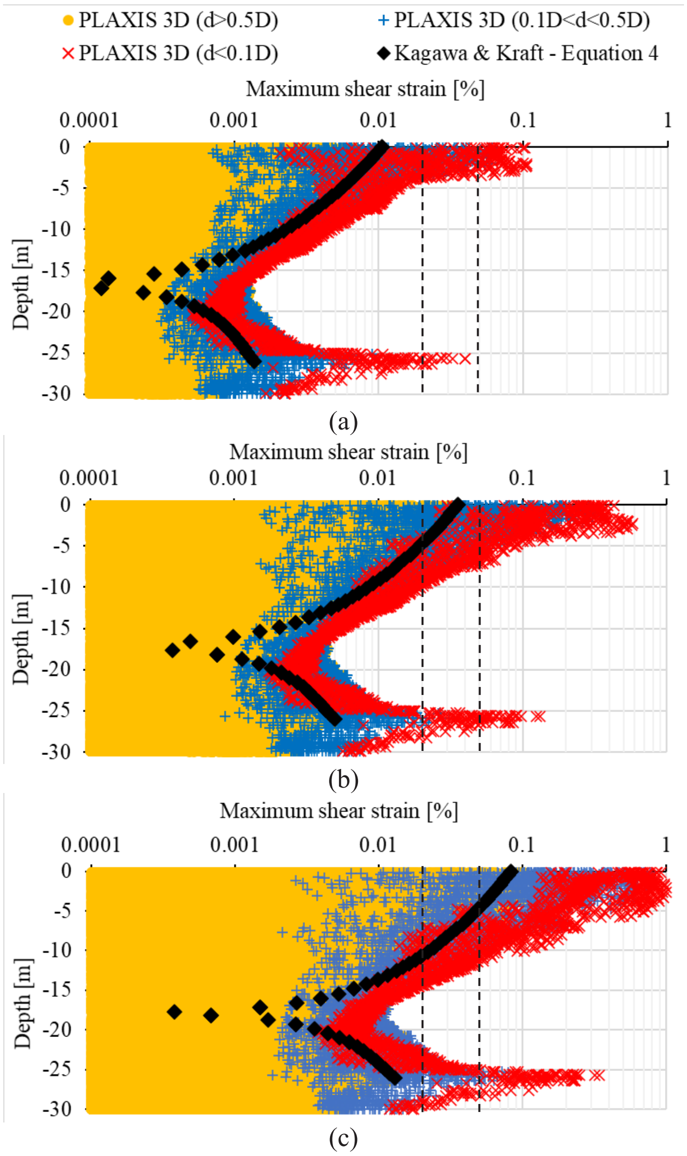

Figure 6. Comparison between shear strains extracted from the 3D FE model and calculated via Equation 4 for mudline deflections equal to (a) 2mm, (b) 6mm and (c) 12mm. Vertical dashed lines indicate the 0.02-0.05% shear strains range

5 Conclusions

Two different methods have been studied in this paper for the soil damping assessments of OWTs, an analytical and a numerical method. Based on the selected input conditions and author's assumptions, the following main conclusions are drawn:

- The obtained soil damping for the examined mudline deflections range (Figure 5), which is typically of interest for the design of OWTs under environmental loading, are in good agreement with values reported in literature (see Section 1), but largely depend on the analysed system and input conditions.
- The applied damping correlations from literature lead to higher soil material damping in comparison with the project-specific calibrated damping curves. This has a direct effect on the obtained values of soil damping. Correlations from literature should be used with caution when results cannot be substantiated with project-specific data. Undoubtedly, the importance of high-quality laboratory test data with as limited disturbance as possible is paramount.
- The results of the analytical method as proposed by Cook & Vandiver (1982) are in very good agreement with the numerical FV results for mudline displacements up to approximately 5mm. Such mudline displacement is typically encountered at FLS conditions. This finding gives confidence that the employed analytical method can be a powerful tool for the fatigue-oriented damping assessment of support structures for large OWTs at the early phases of the design. Additional case studies and validation on a project-specific basis is required to gain better understanding about the method's limitations and confidence in its application.
- For mudline displacement higher than approximately 5mm the results of the FV method should be treated with caution as they become progressively questionable. This is due to the constitutive formulation of the HSsmall model which leads to unrealistically high soil material damping (see Section 3.2.2). A constitutive model with more advanced damping formulation should be used to draw conclusions regarding soil damping at higher displacement levels.
- Scour-related effects, in the form of either local/global scour or presence of a scour protection system, are not accounted for in this study. Nonetheless, it is highlighted that both situations may have a considerable impact on the soil damping results. It is therefore important to consider scour-related effects in the detailed phase of the design or when at-

tempting validation of numerical models against data measured in the field.

6 Acknowledgments

The authors acknowledge the contribution of Dr. M. Seidel, Dr. S. Schafhirt and M. Brommundt to the conceptualisation of the presented study and the discussions on the evaluation of the obtained results.

7 References

Alpan, I. (1970). The geotechnical properties of soils. Earth-Science Reviews, 6(1), 5-49.

Baldi, G., Bellotti, R., Ghionna, V., Jamiolkowski, M., Pasqualini, E. (1986). Interpretation of CPT's and CPTU's. 2nd Part: Drained Penetration. In Proc. 4th International Geotechnical Seminar, Singapore, pp- 143 – 156.

Brinkgreve, R. B. J., Kappert, M. H., & Bonnier, P. G. (2007). Hysteretic damping in a small-strain stiffness model. Proc. of Num. Mod. in Geomech., NUMOG X, Rhodes, 737-742.

Brinkgreve, R.B.J., Kumarswamy, S., Swolfs, W.M., Fonseca, F., Ragi Manoj, N., Zampich, L., Zalamea, N. (2021). PLAXIS manual v21.01. Plaxis bv – a Bentley Systems company, Delft, the Netherlands.

Byrne, B., Burd, H., Zdravkovic, L., Abadie, C., Houlsby, G., Jardine, R., Martin, C., McAdam, R., Pacheco Andrade, M., Pedro, A., Potts, D., Taborda, D. (2019). PISA design methods for offshore wind turbine monopiles. In: Proc. OTC - Offshore Technology Conference, OTC-29373-MS. Houston, Texas. http://dx.doi.org/10.4043/29373-MS.

Carswell, W., Johansson, J., Løvholt, F., Arwade, S. R., Madshus, C., DeGroot, D. J., & Myers, A. T. (2015). Foundation damping and the dynamics of offshore wind turbine monopiles. Renewable Energy, 80, 724-736. https://doi.org/10.1016/j.renene.2015.02.058

Chen, C., & Duffour, P. (2018). Modelling damping sources in monopile-supported offshore wind turbines. Wind Energy, 21(11), 1121-1140. https://doi.org/10.1002/WE.2218

Chopra A. K. (1995). Dynamics of structures: theory and applications to earthquake engineering. Prentice Hall, Englewood Cliffs, N.J.

Cook, M.F., Vandiver, J.K. (1982) Measured and Predicted Dynamic Response of a Single Oil Platform to Random Wave Excitation, OTC 4285.

Damgaard M, Andersen J, Ibsen L, Andersen L (2013). Time-varying dynamic properties of offshore wind turbines evaluated by modal testing. In: Proceedings of the 18th international conference on soil mechanics and geotechnical engineering (ICSMGE2013). International Society of Soil Mechanics and Geotechnical Engineering (ISSMGE).

Damgaard, M., Andersen, L. V., & Ibsen, L. B. (2015). Dynamic response sensitivity of an offshore wind turbine for varying subsoil conditions. Ocean Engineering, 101, 227-234. https://doi.org/10.1016/j.oceaneng.2015.04.039

Darendeli, M. B. (2001). Development of a new family of normalized modulus reduction and material damping curves. PhD thesis, the university of Texas at Austin.

DNV (2019). DNV-RP-C212. Offshore soil mechanics and geotechnical engineering. Recommended Practice. Det Norske Veritas (DNV). Ed. September 2019.

DNV (2021). DNV-ST-0126. Support structures for wind turbines. Standard. Det Norske Veritas (DNV). Ed. December 2021.

IEC (2019). IEC 61400-3-1. Wind energy generation systems - Part 3-1: Design requirements for fixed offshore wind turbines. International Electrotechnical Commission (IEC). Ed. April 2019.

Ishihara, T, Wang, L. (2019). A study of modal damping for offshore wind turbines considering soil properties and foundation types. Wind Energy, 22: 1760– 1778. https://doi.org/10.1002/we.2401

Kagawa, T., & Kraft, L. M. (1980). Lateral load-deflection relationships of piles subjected to dynamic loadings. Soils and Foundations, 20(4), 19-36.

Kementzetzidis, E., Corciulo, S., Versteijlen, W. G., & Pisanò, F. (2019). Geotechnical aspects of offshore wind turbine dynamics from 3D non-linear soil-structure simulations. Soil Dynamics and Earthquake Engineering, 120, 181-199. https://doi.org/10.1016/j.soildyn.2019.01.037

Lysmer, J. and Kuhlemeyer, R. L. (1969) Finite Dynamic Model for Infinite Media. J. Engineering Mechanics Division, 95, 859-878.

Malekjafarian, A., Jalilvand, S., Doherty, P., & Igoe, D. (2021). Foundation damping for monopile supported offshore wind turbines: A review. Marine Structures, 77. https://doi.org/10.1016/j.marstruc.2021.102937

Mayne, P.W., Rix, G.J. (1993). G_{max} – q_c Relationships for Clays. Geotechnical Testing Journal. Vol. 16, No. 1, pp. 54-60.

Panagoulias, S., de Winter, C., Navalkar, S. T., & Nernheim, A. (2023). Sensitivity of the seismic response of monopile-supported offshore wind turbines to soil variability. Ocean Engineering, 268, 113545. https://doi.org/10.1016/j.oceaneng.2022.113545

Robertson, P.K., Cabal, K.L. (2015). Guide to Cone Penetration Testing for Geotechnical Engineering. 6th edition. Signal Hill.

Rix, G.J., Stokoe, K.H. (1991). Correlation of Initial Tangent Modulus and Cone Penetration Resistance. In: Proc. 1st International Symposium on Calibration Chamber Testing ISOCCTI, 351-362.

Rollins, K. M., Evans, M. D., Diehl, N. B., & III, W. D. D. (1998). Shear modulus and damping relationships for gravels. Journal of geotechnical and Geoenvironmental Engineering, 124(5), 396-405.

Schafhirt, S., Page, A., Eiksund, G. R., & Muskulus, M. (2016). Influence of soil parameters on the fatigue lifetime of offshore wind turbines with monopile support structure. Energy Procedia, 94, 347-356. https://doi.org/10.1016/j.egypro.2016.09.194

Schmertmann, J.H. (1978). Guidelines for Cone Penetration Test; Performance and Design. U.S. Department of Transportation. FHWA, Washington D.C. FHWA-TS-78-209.

Seed, H. B., Wong, R. T., Idriss, I. M., & Tokimatsu, K. (1986). Moduli and damping factors for dynamic analyses of cohesionless soils. Journal of Geotechnical Engineering, 112(11), 1016-1032.

Stuyts, B., Weijtjens, W., Devriendt, C. (2022). Revised Soil Damping Using Realistic Pile-Soil Interaction Models. In Proc. 2nd Vietnam Symposium on Advances in Offshore Engineering. VSOE2021, vol 208. Springer, Singapore. https://doi.org/10.1007/978-981-16-7735-9_49

Vucetic, M., Dobry, R. (1991). Effect of Soil Plasticity on Cyclic Response. Journal of Geotechnical Engineering. Vol. 117, Issue 1 (January 1991). https://doi.org/10.1061/(ASCE)0733-9410(1991)117:1(89)

Watanabe, K., Pisanò, F. & Jeremić, B (2017). Discretization effects in the finite element simulation of seismic waves in elastic and elastic-plastic media. Engineering with Computers 33, 519–545. https://doi.org/10.1007/s00366-016-0488-4